05

Resistance of a carbon-carbon composite to high-rate deformation and fracture under shock wave loading

© A.R. Gareev,[1] G.V. Garkushin,[2] V.M. Mochalova,[2] S.V. Razorenov,[2] A.S. Savinykh,[2] A.V. Utkin[2]

[1] State Research Institute of Graphite-Based Structural Materials „NII graphite“,
111524 Moscow, Russia
[2] Federal Research Center for Problems of Chemical Physics and Medical Chemistry, Russian Academy of Sciences,
142432 Chernogolovka, Moscow region, Russia
e-mail: utkin@icp.ac.ru

Received July 4, 2025
Revised December 3, 2025
Accepted December 3, 2025

The shock compressibility, shock wave structure, and spall strength of a unidirectional carbon-carbon composite material (CCCM 1-D) have been determined for shock wave propagation at angles of 0°, 45°, and 90° relative to the fiber orientation. Free-surface velocity profiles and particle velocity profiles at the sample/water-window interface were recorded using a VISAR laser interferometer, with simultaneous measurement of shock wave velocities. A two-wave front structure was observed for shock wave propagation at 0° and 45°. The dependences of the shock Hugoniot and spall strength on the shock loading direction have been established. A distinct kink in the Hugoniot curve at a shock pressure of approximately ~ 30 GPa provides evidence of a phase transition in carbon. It is shown that the composite does not undergo fracture within the elastic deformation regime, and its spall strength is governed by the dynamic elastic limit, exceeding 1 GPa. Under plastic deformation, the CCCM 1-D specimen loses its elastic properties, and the spall strength decreases by an order of magnitude irrespective of fiber orientation.

Keywords: carbon-carbon composite, shock wave, Hugoniot equation of state, dynamic elastic limit, spall strength.

DOI: 10.61011/TP.2026.04.63262.169-25

Introduction

Composite materials with a carbon matrix are applied in industry due to variability of effective properties. Their kind and properties depend on a crystal structure depending on conditions of matrix synthesis (from a gas phase, a liquid phase), porosity at all size levels of the material, contact conditions. Depending on their purpose, thermal conductivity of these materials varies from 0.15 W/(m·K) for thermal protection to 1200 W/(m·K) in case of being applied in structures with active heat removal. The carbon-matrix composites are applied in missile engineering and the most complicated type of loading for them during operation may be considered to be a thermal impact, wherein thermal conductivity is one of the characteristics determining performance of the material. Taking into account high rates of effect by thermal flows, evaluation of occurring states of a material, including evaluation of probability of a shock wave, requires correct physical models based on experimental data obtained in conditions that are the most suitable for numerical calculations. An undisputable advantage in this respect belongs to shock-wave research methods that make it possible to realize one-dimensional deformation of materials, which is strictly analyzed under basic conservation laws.

The composites based on fibers of a various structure and chemical composition are characterized by high anisotropy of the properties and their response to external effect greatly varies depending on a filling degree, a binder type [1–4], a microstructure, porosity [5–8] and other special features of their fabrication [9–11]. The carbon-matrix composite materials are not designed to vary a reinforcing filler by a chemical composition (usually, the filler is carbon in the form of continuous or short fibers), since a technique of carbon-matrix fabrication involves processes of thermal treatment at the temperatures above 2000 °C. At the same time, both the carbon filler and the carbon matrix have significant variation of physical-mechanical and thermal-physical properties, which is inherited at a crystal structure level from a precursor used for carbon production. If this composite material is considered at a microstructure level, then variability of fabrication of reinforcing structures is limited only by existing technologies — winding of carbon filaments, multi-dimensional weaving, arrangement, chaotic filling with short filaments, production of the reinforcing filler from carbon tissues. Reliably proven under conditions of the thermal impact are carbon-matrix composite materials reinforced with carbon filaments in at least three directions [12].

Recent decades have seen a large number of studies that experimentally and theoretically address behavior of composite materials based on carbon, glass, aramid fibers, ultra-high-molecular-weight polyethylene and other fibers under effect of a shock wave [2,4,8,13]. It includes investigation of fibers in various matrices, such as epoxy resin, cyanate ester, phenolic resin, polyvinylchloride [14–19] and study of

properties of the very matrices and matrices with inclusion of various additives [20–25]. Most experimental data about dynamic properties of the fiber-reinforced composites under high pressure can be found for a case when the shock wave propagates perpendicular to the fibers (90°), while a smaller number of the studies provides data for shock-wave loading along the fibers (0°) and at various angles to a direction of propagation of the shock wave [5,9,10,26–30]. Authors of the study [9] provided experimental profiles, when the shock wave propagates across a unidirectional composite at various angles to a reinforcing direction. It was demonstrated that an elastic precursor to be followed by the propagating shock wave was formed at 5 and 15°. In case of the impact at 45° the elastic precursor is transformed into a plastic wave with a diffuse front. For orientation of 90° a single shock wave is recorded. The similar results were obtained by other authors, for example, [5,26,27,29,30] when studying the composites along and across the fibers — the specimens of 0° exhibited a two-wave structure, while for the perpendicular direction the single shock wave was recorded. The same structure of the shock wave for the two fiber orientations (0 and 90°) was obtained in our previous studies for the composites based on unidirectional aramid and carbon fibers [7,31] and woven aramid- and carbon-epoxy composites [8,32].

The experimental data obtained by the various authors indicate an individual reaction of the composite materials under effect of the shock wave. In this situation, it is important to experimentally study the composites based on fiber of different nature in order to reveal general patterns of their deformation and fracture under high dynamic pressures. The present study is aimed at experimentally determining a shock Hugoniot and spall strength of the carbon-carbon composite material (CCCM 1-D) with various fiber orientation in relation to the direction of propagation of the shock wave.

1. Structure of the carbon-carbon composite specimen and experimental setup

Fig. 1 shows photos of the microstructure of the studies specimens. The composite material is structured as carbon rods on a UKN/5000 fiber of the diameter (1.17 ± 0.3) mm, which are arranged in one direction, with subsequent filling of space between them with carbon pitch that is used as a raw material for producing carbon fibers. The 3.5 mm-thick plane-parallel specimens for the shock-wave experiments were cut by the electroerosion method with subsequent surface treatment (grinding and polishing) out of a single 30 mm-diameter cylindrical blank. At the same time, the blank was cut along a generatrix for producing the specimens in tests with a transverse fiber direction. It should be noted that when loading across the fibers the specimen includes at most three rods along a direction of propagation of the shock wave. It is not possible to experimentally check

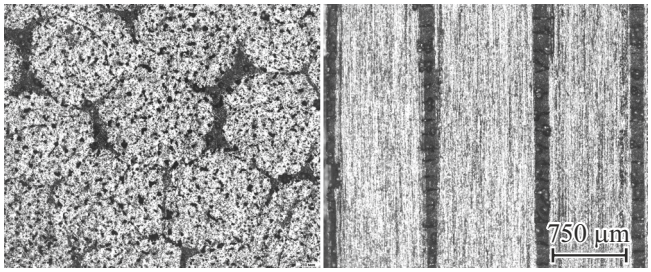

Figure 1. Microstructure of the carbon-carbon composite CCCM 1-D perpendicular to the fibers (loading along the fibers) and along the fibers (loading perpendicular to the fibers).

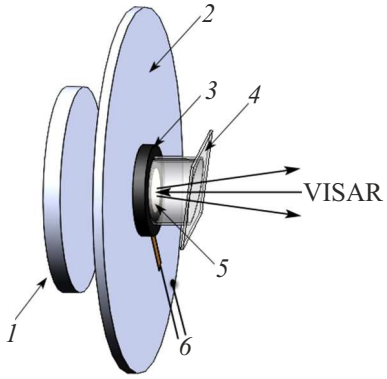

Figure 2. Experimental setup: *1* — the impactor, *2* — the baseplate, *3* —- the specimen, *4* — the water window, *5* — the aluminum foil, *6* — the polarization gauge.

influence of the thickness on the obtained results due to a limited diameter of the initial cylindrical blank. Therefore, in order to ensure a one-dimensional nature of flowing, the maximum specimen thickness could not exceed 3.5 mm.

The density was measured using hydrostatic weighing and it was 1.84 g/cm^3. Since the composite is anisotropic, the speed of sound depends on a wave propagation direction. It was measured using an ultrasound technique (MG-NIVP „Akustika“) that was used to obtain the following values: the longitudinal speed of sound cl along the fibers was 11.44 km/s, so was 1.90 km/s when being perpendicular to the fiber direction, at the angle 45° — 7.98 km/s.

The experimental setup for determining shock compressibility (a shock Hugoniot) of the carbon-carbon composite is shown in Fig. 2. The impactors *1* were accelerated by explosion propellant devices. The shock waves in the studied specimens *3* were formed by collision of the 90 mm-diameter aluminum impactor *1* accelerated by explosion products to the velocity Wi, with the baseplate *2*. The VISAR interferometer [33] was used to measure the velocity of a specimen/water interface *4*. Probing radiation was reflected from the 7 μm-thick aluminum foil *5* glued to the specimen. In order to determine an absolute value of the velocity, reflected radiation was simultaneously recorded by two interferometers with various references of an optical

delay line. In each test, the polarization gauge *6* recorded a time of entry of the shock wave into the specimen, which made it possible to determine the value of the wave velocity D with an error at most $\pm 0.5\,\%$ using the interferometric data.

In order to determine spall strength and Hugoniot elastic limit of CCCM 1-D, the 2 mm-thick impactors made of PMMA or aluminum were accelerated within the velocity range 190−350 m/s by a 50 mm-caliber gas gun. The velocity and a skew of the impactors were recorded by electric-contact pins. A gun barrel and space around the specimen were vacuumed before the experiment. The higher pressures were obtained by accelerating the 3.3- and 7 mm-thick impactors by means of explosion devices to the velocities (650 ± 30) m/s and (1100 ± 50) m/s, respectively.

2. Structure of the shock-wave front

Parameters of experimental assemblies and results of the experiments of studying the front structure with the various fiber orientation in relation to the shock-wave propagation direction are given in Table 1 and Fig. 3. Table includes a velocity of the aluminum impactor W_i, its thickness h_i, a material and thickness of the baseplate h_b and a specimen thickness h_s. Designations of the velocity profiles shown in Fig. 3 coincide with numbering of the experiments in Table 1. No water window was in these tests.

When the CCCM 1-D is loaded perpendicular to the fiber direction (the dependence $1p$ in Fig. 3), it is recorded in the profile $u_{fs}(t)$ that only the single wave exits to the specimen surface. No sign of formation of a two-wave configuration is observed, since the wave velocity significantly exceeds the measured c_l. After reaching the maximum value, the free surface velocity remains the same during the entire period of recording. A specific feature that is observed directly behind the shock-wave front up to the time point

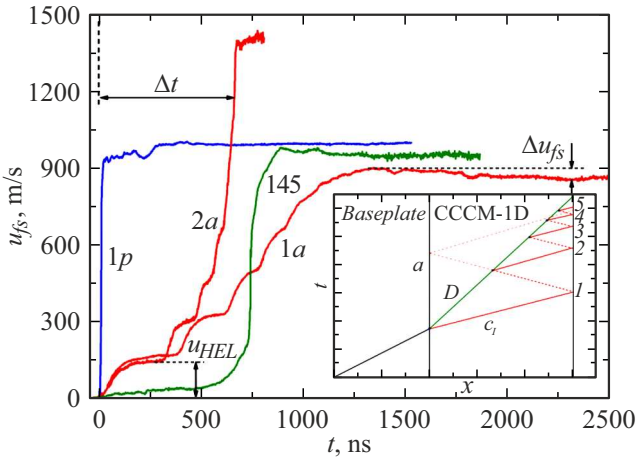

Figure 3. Velocity profiles of the free surface of the 1-D specimens in longitudinal ($1a$, $2a$) and transverse ($1p$) fiber orientation as well as at the angle of 45° (145). The profiles have the numbers of the experiments marked as per Table 1.

Table 1. Parameters of shock loading of the specimens when determining the front structure

№ of the experiment	Impactor velocity, W_i, m/s	Impactor thickness, h_i, mm	Baseplate thickness, h_b, mm	Specimen thickness, h_s, mm
Loading along fibers				
$1a$	650 ± 20	3.37	3.37	3.00
$2a$	1100 ± 30	7.00	7.00	3.00
Loading perpendicular to fibers				
$1p$	650 ± 20	3.30	3.30	3.01
Loading at 45° to fibers				
145	650 ± 20	3.30	2.00	2.98

~ 300 ns is related to inhomogeneities of the specimen microstructure.

When CCCM 1-D is loaded along the fibers (the dependences $1a$, $2a$ in Fig. 3), the two-wave configuration is formed in the studied specimen, which is often referred to as elastic-plastic one similar to metals. Interaction of the elastic-plastic compression wave with the specimen's free surface results in origination of reflections and distortion of the recorded wave profile [34,35]. Appearing wave interactions corresponding to the test $1a$ are shown in a diagram time t — the x coordinate in an insert in Fig. 3. A trajectory of propagation of the plastic wave is designated as D and the red color marks characteristics along which the sound waves c_l propagate. It includes only the characteristics that are used with further discussion of results. After exiting to the free surface, the first (elastic) wave propagating with the longitudinal speed of sound c_l (the respective moment of time is designated by a digit in the insert of Fig. 3) is reflected by a rarefaction wave. After the reflected wave encounters the plastic shock wave, an elastic compression wave is again formed in the unloaded material, which can be regarded as reflection of the elastic rarefaction wave from the plastic compression wave. This reflections forms the second step on the velocity profile of the free surface (the point *2*). As a result of multiple re-reflections, a „step-wise" increase of the velocity of the free surface is observed (the points *1*−*5*). Since the longitudinal speed of sound c_l along the fibers is 11.44 km/s, the two-wave configuration will be observed in the wide pressure range until the velocity of the plastic way exceeds c_l.

Fig. 3 also shows the velocity profile of the free surface of the CCCM 1-D under shock loading of the specimen at the angle of 45° to the fiber direction (the experiment No. 145). In this case, in the same way as at orientation of 0°, exit of the elastic and the plastic wave to the free surface is recorded. However, under loading at the angle of 45° the elastic wave is smeared and the step-wise nature of

the velocity increase is not observed clearly. Besides, the precursor amplitude is much smaller than in the test 1a.

The elastic compression wave amplitude u_{HEL}, which is measured from the wave profile, makes it possible to calculate Hugoniot elastic limit $\sigma_{HEL} = 1/2 \cdot \rho_0 \cdot c_l \cdot u_{HEL}$, which is related to dynamic elastic limit of the material [36]. In longitudinal fiber orientation, the value of σ_{HEL} of CCCM 1-D varies from experiment to experiment and is 1.78 GPa in the test 1a and is 1.54 GPa in the test 2a. This difference is not related to influence of the maximum compression stress on the value of σ_{HEL}, but caused by a heterogeneous structure of the specimens. At orientation of 45°, the value $u_{HEL} = 41$ m/s taken on the profile $u_{fs}(t)$ is an estimated one, while its respective value of dynamic elastic limit is 0.30 GPa.

3. Shock compressibility of the carbon-carbon composite

The parameters of the experimental assemblies and the results of the experiments for studying shock-wave compressibility and the unidirectional carbon-carbon composite are given in Table 2 and Fig. 4–7. Unlike the tests whose results are shown in Fig. 3, in this case the velocity profiles were measured at the specimen/water contact interface. The designations in Table 2 are similar to the designations in Table 1. Besides, it also contains the measured shock wave velocity D, the pressure P and the particle velocity u. The pressure and the particle velocity were calculated by the measured values of W_i, D and the known shock Hugoniots of the baseplate and the impactor as a result of analysis of flowing in the plane P-u [32]. Designations of the velocity profiles shown in Fig. 4–7 coincide with numbering of the experiments in Table 2.

Along with the velocity profiles at the specimen/water interface, Fig. 4–7 also shows velocity profiles measured in separate experiments at the baseplate/water interface

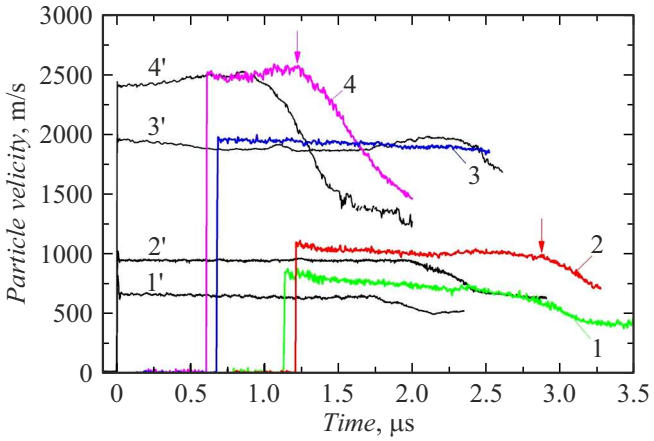

Figure 4. Particle velocity profiles at the specimen/water interface with transverse fiber orientation and at shock compression pressure below 30 GPa. Numbering of the profiles corresponds to Table 2.

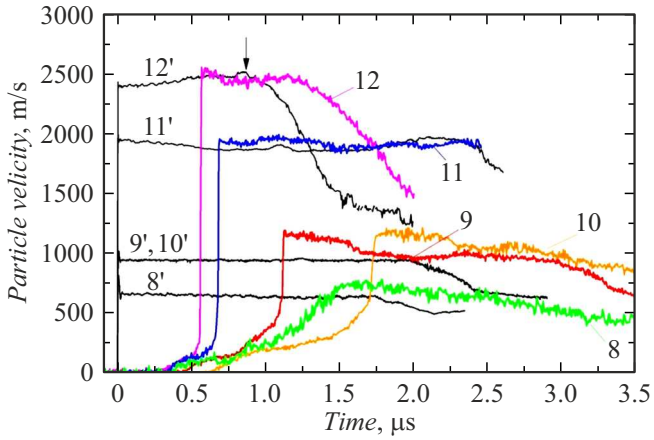

Figure 5. Particle velocity profiles at the specimen/water interface with longitudinal fiber orientation and at shock compression pressure below 30 GPa. Numbering of the profiles corresponds to Table 2.

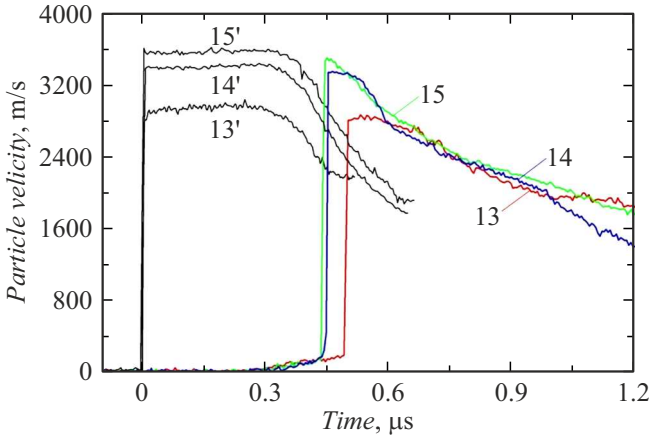

Figure 6. Particle velocity profiles at the specimen/water interface with longitudinal fiber orientation and at shock compression pressure above 30 GPa. Numbering of the profiles corresponds to Table 2.

without the specimen. The make it possible to determine amplitudes and durations of the shock waves that enter the specimens. The digital designations 1′–18′ correspond to the entering wave profiles in the tests 1–18.

The experimentally used impactors form compression pulses, in which after a shock jump the velocity remains approximately constant for the period of time from 0.3 to 2 μs, which is determined by arrival of rear unloading from the impactor. As it propagates across the specimen, this time is shortened, but since the specimen thickness is small, all the tests by the moment of output of the wave to the water interface an area of constant values of the parameters is preserved until arrival of the rarefaction wave from the impactor. Fig. 4, 5 marks this time for several profiles with vertical arrows. Since a start of the velocity drop is not always clear on the obtained profiles, the position of the

Table 2. Parameters and results of the experiments when determining the shock Hugoniot of the unidirectional carbon-carbon composite with longitudinal and transverse fiber orientation as well as at the angle of 45° in relation to the impact direction

Experiment №	Impactor velocity, W_i, km/s	Impactor thickness, h_i, mm	Baseplate thickness, h_b, mm	Specimen thickness, h_s, mm	Shock wave velocity, D, km/s	Particle velocity, u, km/s	Pressure, P, GPa
Loading perpendicular to fibers							
1	1.13	7	Cu, 5.5	3.39	2.99 ± 0.05	0.59 ± 0.02	3.24 ± 0.05
2	1.13	7	Al, 4.0	4.47	3.72 ± 0.05	0.79 ± 0.02	5.40 ± 0.05
3	2.50	10	Al, 4.0	3.40	4.97 ± 0.05	1.64 ± 0.02	14.96 ± 0.05
4	3.30	5	Al, 2.0	3.40	5.69 ± 0.05	2.11 ± 0.02	22.04 ± 0.05
5	5.05	2	Cu, 2.0	3.00	6.50 ± 0.05	2.54 ± 0.02	30.31 ± 0.05
6	4.60	2	Al, 2.0	2.44	6.80 ± 0.05	2.86 ± 0.02	35.71 ± 0.05
7	5.05	2	Al, 2.0	2.58	7.08 ± 0.05	3.14 ± 0.02	40.82 ± 0.05
Loading along fibers							
8	1.13	7	Cu, 5.5	3.40	2.57 ± 0.05	0.57 ± 0.02	4.65 ± 0.05
9	1.13	7	Al, 4.0	3.43	3.07 ± 0.05	0.76 ± 0.02	5.50 ± 0.05
10	1.13	7	Al, 4.0	5.47	3.07 ± 0.05	0.76 ± 0.02	5.50 ± 0.05
11	2.50	10	Al, 4.0	3.42	5.02 ± 0.05	1.64 ± 0.02	15.12 ± 0.05
12	3.30	5	Al, 2.0	3.36	5.92 ± 0.05	2.09 ± 0.02	22.72 ± 0.05
13	5.05	2	Cu, 2.0	3.42	6.95 ± 0.05	2.52 ± 0.02	32.16 ± 0.05
14	4.60	2	Al, 2.0	3.43	7.52 ± 0.05	2.77 ± 0.02	38.24 ± 0.05
15	5.05	2	Al, 2.0	3.42	7.77 ± 0.05	3.04 ± 0.02	43.37 ± 0.05
Loading at 45° to the fiber direction							
16	1.13	7	Al, 4.0	3.47	3.62 ± 0.05	0.79 ± 0.02	5.58 ± 0.05
17	2.50	10	Al, 4.0	3.19	5.45 ± 0.05	1.60 ± 0.02	16.01 ± 0.05
18	5.05	2	Al, 2.0	3.31	8.07 ± 0.05	3.00 ± 0.02	44.45 ± 0.05

arrows is determined with an error ± 10 ns. In some tests (for example, No. 3), velocity recording stops before arrival of the rarefaction wave.

As in recording the velocity of the free surface (Fig. 3), the most pronounced specific feature of the velocity profiles in longitudinal fiber orientation is presence of the two-wave configuration (Fig. 5, 6). Presence of the water window results in smoothing of the step-wise nature of the velocity increase, which is due to circulation of the precursor between the specimen/water interface and the front of the plastic wave that propagates at the velocity D. In all the performed experiments, the value of D did not exceed 8 km/s, Therefore, during longitudinal fiber orientation the two-wave configuration is observed within the entire measured range of the shock compression pressures up to 40 GPa.

The nature of evolution of the two-wave configuration clearly demonstrates comparison of the tests No. 9 and No. 10 (Fig. 5), which are performed in the same formulation, and only the specimen thickness varied from 3.43 mm in the test 9 to 5.47 mm in the test 10. Divergence between the front of the second wave and the precursor increases as they propagate across the specimen. At the same time, the velocity of each of the waves remains constant.

The velocity profiles at fiber orientation of 45° are shown in Fig. 7. As in longitudinal fiber orientation, the two-wave structure is recorded in this case: first, the water interface is hit by the precursor and then the second shock wave. As already noted when discussing Fig. 3, the existing differences are quantitative, for example, the precursor amplitude decreases. Reduction of the longitudinal speed of sound ($c_l = 7.98$ km/s) results in disappearance of the two-wave configuration in the test No. 18, in which the shock wave velocity D is 8.07 km/s, thereby exceeding c_l.

As already noted, the shock wave velocity D was measured in all the experiments. Since the impactor velocity

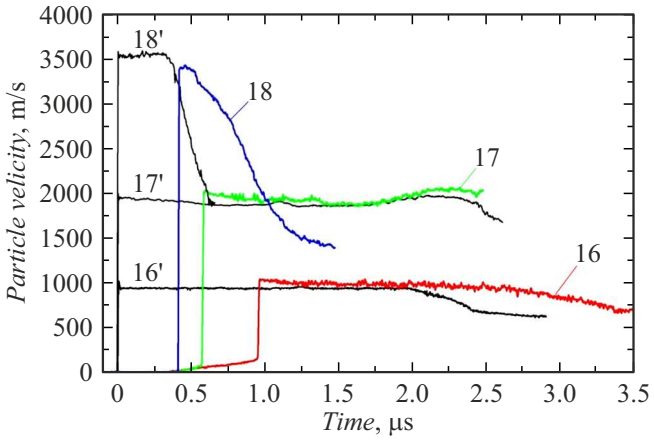

Figure 7. Particle velocity profiles at the specimen/water interface with fiber orientation at the angle of 45°. Numbering of the profiles corresponds to Table 2.

as well as the shock Hugoniots of the impactor and the baseplate are known, it makes it possible to determine the particle velocity u in the studied specimen. Processing of the experimental data results in plotting of the shock Hugoniots of the unidirectional carbon-carbon composite at transverse, longitudinal and 45° fiber orientation in relation to the direction of propagation of the shock wave (Fig. 8). It is clear from comparing the shock Hugoniots at various fiber orientation that compressibility of the specimen depends on the direction of propagation of the shock wave: the shock Hugoniots in the plane D-u have a different slope and intersect when $u \approx 1.6$ km/s for transverse and longitudinal orientations. The second specific feature is presence of a pronounced kink on the dependences $D(u)$ around $u = 2.5-2.8$ km/s, which is due to a graphite/diamond phase transition. These kinks of the shock Hugoniots are marked by vertical arrows (Fig. 8) and their position depends on fiber orientation in relation to the direction of propagation of the shock waves. The obtained result complies with data of the authors [37,38], who demonstrated that under shock-wave loading conditions and kinetics of the carbon/diamond phase transition are very sensitive to a specific structure of original graphite specimens.

It is clear in Fig. 8 that at the specified fiber orientation the experimental data are not approximated by a single linear dependence in the studied pressure range. With transverse fiber orientation $D = 2.17 + 1.7 \cdot u$ when $u < 2.5$ km/s; with longitudinal one — $D = 1.34 + 2.22 \cdot u$, when $u < 2.8$ km/s and at 45° $D = 1.88 + 2.22 \cdot u$ when $u < 2.6$ km/s.

Only three points are obtained on the shock Hugoniot of the composite CCCM 1-D at fiber orientation of 45° . Therefore, it was assumed during approximation of the shock Hugoniot that the phase transition occurred in the same pressure interval as for the other two orientations — approximately when $u = 2.6$ km/s. At the same time, two points below the phase transition lie with good accuracy on the straight line that is parallel to the shock Hugoniots for longitudinal fiber orientation (Fig. 8).

The above-obtained structure of the wave profiles for the carbon-carbon composite CCCM 1-D was considered under an elastic-plastic model, which makes it possible to explain basic patterns of flowing to be realized under shock-wave loading. However, it should be noted that several specific features recorded at the velocity profiles do not comply with this assumption. For example, in the experiments 9 and 10, whose results are given in Table 2 and Fig. 5, the velocity behind the front of the plastic wave remains almost constant for $\sim 0.5\,\mu$s and then abruptly decreases approximately by 100 m/s. Nothing like this is observed in the test 2 (Table 2 and Fig. 4) performed in the same formulation with transverse fiber orientation. This specific feature originates due to the elastic rarefaction wave, which formed after reflection of the precursor from the specimen/water interface. After encountering the plastic front, this wave propagates across the specimen towards the baseplate by the rarefaction wave, which is shown in the insert of Fig. 3 by a thin dashed line. After reflection from the baseplate, it returns to the window interface, causing the velocity drop. If assuming (as done in the insert in Fig. 3) that behind the front of the plastic shock wave the studied medium retains the elastic properties, then the wave reflected from the baseplate shall exit to the window interface in the tests 9 and 10 earlier than the front of the plastic wave. At the same time, the similar situation shall be implemented in the test 1a, too. But no specific feature before the plastic front is observed in these tests. Moreover, if behind the front of the plastic wave the specimen retains the elastic properties, then the wave reflected from the baseplate will be a compression wave, since in the elasticity area dynamic impedance of CCCM 1-D is higher than that of the aluminum baseplate. Therefore, when this wave exits to the window interface

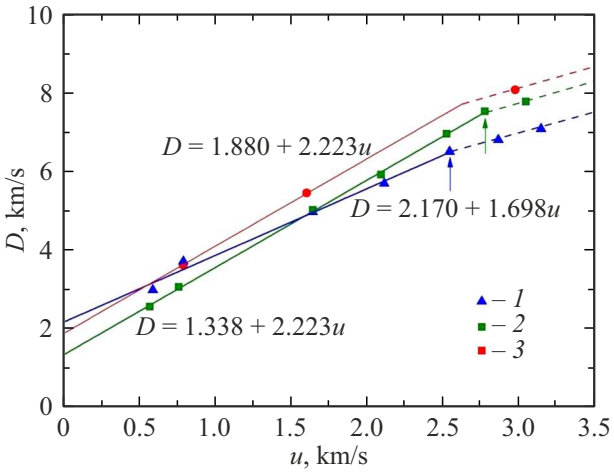

Figure 8. Shock Hugoniots of the unidirectional carbon-carbon composite at transverse fiber orientation (*1*), longitudinal one (*2*) and at the angle of 45° (*3*). Lines mark linear approximation of the experimental data.

an increase of the velocity shall be observed rather than its reduction. These discrepancies to the obtained experimental data are eliminated, if considering that behind the front of the second (plastic) shock wave the carbon-carbon composite CCCM 1-D loses elastic properties. First of all, in this case impedance of CCCM 1-D in the area of plastic deformation is smaller than that of aluminum and, therefore, the wave reflected from the baseplate will be a rarefaction wave and at the moment of its exit to the window interface the velocity of the interface will be reduced. Secondly, time of circulation of this wave across the specimen will increase, since in the area of plastic deformation it will propagate at the velocity that is below the longitudinal speed of sound c_l. The respective value of a Lagrangian speed of sound C_L behind the front of the plastic wave can be obtained from analysis of the wave profiles 9 and 10 (Fig. 5) and is ~ 5.5 km/s, which is much smaller than c_l.

Thus, analysis of shock-wave interactions shall take into account that the studied specimens can lose the elastic properties behind the second (plastic) compression wave.

4. Spall strength of CCCM 1-D

Dynamic strength of the carbon-carbon composite CCCM 1-D was studied by analysis of spallation phenomena during reflection of a compression pulse from the free surface of the medium, at which the compression wave turns into the tension wave [36]. The experimental studies [36,39,40] show that a range of tensile stresses includes nucleation of a large number of microcracks, which in their further development merge into a single main crack that separates the specimen into two parts, with formation of a spallation plate. Parameters of the experimental assemblies and results of the experiments are given in Table 3. Table 3 shows the results of all the experiments, which included recording of the velocity of the free surface, including those provided in Table 1. Along with the previously introduced designations, Table 3 is supplemented with σ_{HEL} — dynamic elastic limit, σ_{sp} — spall strength or maximum tensile stresses in the elastic area of deformation and $\dot{V}/V_0$ — the strain rate in the rarefaction wave before fracture.

The tensile stresses inside the specimen result from interaction of the rarefaction wave reflected from the free surface with an incident rarefaction wave that propagates into the specimen from a rear side of the impactor. In Fig. 3 these conditions are implemented only in the experiment $1a$, in which reaching of the maximum velocity is followed by recording of a drop of the latter, which is related to free surface exit of the unloading wave arriving from the rear surface of the impactor. Interaction of the latter with the reflected plastic wave from the free surface of CCCM 1-D in the form of the rarefaction wave results in spall fracture. The magnitude of the surface velocity drop Δu_{fs} (Fig. 3) from its maximum to the first minimum before the front of the spallation pulse is

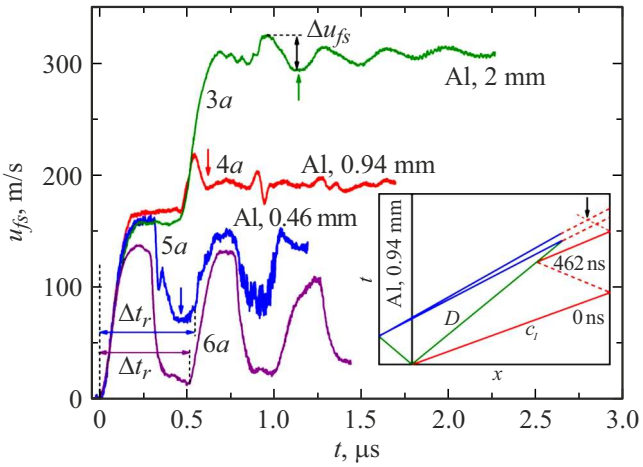

Figure 9. Velocity profiles of the free surface of the CCCM 1-D specimens being loaded by the variously-thick aluminum impactors with the velocity of 350 m/s along the fibers ($3a-5a$) and the experiment ($6a$), in which the maximum compression stress did not exceed σ_{HEL}. The profiles are provided with impactor thicknesses, time moments of implementation of the maximum tensile stresses and numbers of the experiments as per Table 3. The insert includes a t–x diagram of wave interactions in the experiment $4a$.

proportional to spall strength of the material σ_{sp}. In a linear approximation, the value of spall strength is determined as $\sigma_{sp} = 1/2 \cdot \rho_0 \cdot c_0 \cdot \Delta u_{fs}$ [41], where c_0 is a volume speed of sound, which takes the value of c_b from the measured dependence $D = c_b + b \cdot u_p$. When loading along the fibers, $c_b = 1.338$ km/s, $\sigma_{sp} = 55$ MPa.

Fig. 9 shows the velocity profiles of the free surface of the 3 mm-thick CCCM 1-D specimens when being loaded by the aluminum impactors of the thickness 2, 0.94 and 0.46 mm with the velocity of 350 m/s along the fibers. All the three experiments record exit of the elastic wave to the free surface. The measured amplitude of the elastic wave u_{HEL} was used to calculate dynamic elastic limit of CCCM 1-D σ_{HEL}; the data obtained are provided in Table 3 and comply with the high-rate experiments $1a$ and $2a$. The experiments $3a$, $4a$ and $5a$ are aimed at measuring spall strength at the various stages of circulation of the elastic wave between the front of the plastic wave and the free surface. The insert of Fig. 9 includes a t–x diagram of wave interactions implemented in the experiment $4a$. A trajectory of propagation of the plastic wave is designated as D and the red color marks characteristics along which the sound waves c_l propagate. The blue color marks a centered rarefaction wave that propagates from the rear surface of the impactor. Unlike the experiment $3a$, in which a quite thick impactor was used, in the experiment $4a$ unloading from the 0.94 mm-thick impactor arrives much earlier. At the same time, the elastic unloading wave has time to reflect from the plastic one once and exit to the free surface as the elastic compression wave at the time of 462 ns. When the unloading wave propagating from the impactor and the

Table 3. Formulation and results of the CCCM 1-D experiments

№ of the experiment	Impactor velocity, W_i, m/s	Impactor thickness, h_i, mm	Baseplate thickness, h_b, mm	Specimen thickness, h_s, mm	Elastic limit, σ_{HEL}, GPa	Spall strength, σ_{sp}, GPa	Strain rate, $\dot{V}/V_0$, s^{-1}
Loading along the fiber direction							
1*a*	650	Al, 3.37	Al, 2.00	3.00	1.78	0.055	$1.94 \cdot 10^4$
2*a*	1100	Al, 7.00	Al, 2.00	3.00	1.54	–	–
3*a*	350	Al, 1.998	–	3.04	1.65	> 0.33	$1.12 \cdot 10^4$
4*a*	350	Al, 0.94	–	3.05	1.76	> 0.33	$2.31 \cdot 10^4$
5*a*	350	Al, 0.462	–	3.03	1.68	> 0.94	$3.91 \cdot 10^4$
6*a*	190	Al, 0.735	–	2.97	–	1.32	$1.62 \cdot 10^5$
Perpendicular to the fiber direction							
1*p*	650	Al, 3.30	Al, 2.00	3.01	0.01–0.015	–	–
2*p*	350	PMMA 1.258	–	2.96	0.01–0.015	0.110	$3.91 \cdot 10^5$
3*p*	190	PMMA 0.961	–	3.06	0.01–0.015	0.036	$0.67 \cdot 10^4$
4*p*	350	PMMA 0.965	–	3.04	0.01–0.015	0.036	$0.82 \cdot 10^4$
Loading at 45° to the fiber direction							
145	650	Al, 3.30	Al, 2.00	2.98	0.30	0.063	$1.79 \cdot 10^4$
245	250	Al, 3.00	–	3.07	0.63	0.071	$1.62 \cdot 10^4$

reflected elastic wave from the free surface interact, tensile stresses originate in the range marked by a vertical arrow in the insert. The similar situation also occurs in the experiment 3*a*, in which the precursor has time to reflect twice. Both the cases have fracture that results, in particular, in typical oscillations of the velocity in the spallation plate. A velocity difference Δu_{fs} between its maximum value and a value before the spallation pulse is 31 m/s in these two tests.

In the experiment 5*a* with the 0.46 mm-thick impactor, the unloading wave catches the plastic wave that totally decays, and an elastic wave exits to the free surface. It is interaction of the two colliding elastic unloading waves that resulted in the tensile stresses. The elastic unloading wave's amplitude Δu_{fs} recorded at the free surface was 89 m/s. Interaction of the elastic waves in the experiment 5*a* is confirmed by the fact that the second re-reflected pulse exits in 523 ns. The velocity of propagation of the wave within the elastic area is determined by exit of the second re-reflected pulse as $2h_s/\Delta t_r = 11.56$ km/s, which insignificantly exceeds the measured c_l.

If assuming that all the wave interactions in the experiments 3*a*, 4*a* and 5*a* occur within the elastic area, then maximum stresses of compression and tension shall be calculated by means of the relationship $\sigma_{sp} = 1/2 \cdot \rho_0 \cdot c_l \cdot \Delta u_{fs}$. In the experiments 3*a* and 4*a*, the maximum tensile stresses were 0.33 GPa, while in the experiment 5*a* they were 0.94 GPa. Such a significant difference of σ_{sp} indicates that the CCCM 1-D samples fracture does not occur in the elastic region, which is probably due to the following circumstances. The plastic wave amplitude decays due to unloading from the impactor in these tests before its exit to the free surface. For this reason, a specimen's part that is adjacent to the free surface is not plastically deformed, retains the elastic properties and can withstand high tensile stresses. But within a plastically-deformed area spall strength is very low as it follows from results of the test 1*a* Therefore, as soon as the tensile stresses at an interface of these two areas exceed this value, it fractures. At the same time, the elastic part of the specimen has much higher stresses originated and they depend on specific conditions of the experiment and make it possible to obtain only a lower estimate of the value of spall strength within the elasticity area.

In order to determine spall strength of the CCCM 1-D specimens in the elasticity area, the test 6*a* (the profile 6*a* in Fig. 9) was performed, in which the maximum compression stress was 1.47 GPa, i.e. it did not exceed σ_{HEL}. No spall fracture occurred in this experiment and the maximum tensile stress was 1.32 GPa. The elastic wave velocity was calculated based on exit of the second re-reflected pulse to show that $2h_s/\Delta t_r = 11.647$ km/s. In this experiment, the elastic wave velocity U_{el} measured by means of contact sensors was 11.627 km/s. Both the values are almost the

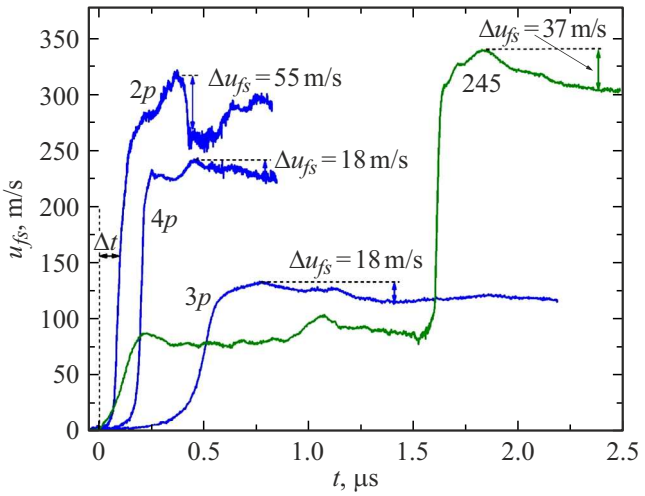

Figure 10. Velocity profiles of the free surface of the CCCM 1-D specimens under shock loading perpendicular to and at the angle ot 45° to the fiber direction. The profiles have the numbers of the experiments marked as per Table 3.

same and insignificantly exceed the measured c_l in the room conditions.

Fig. 10 shows the velocity profiles of the free surface of the 3 mm-thick CCCM 1-D specimens under shock loading perpendicular to the fiber direction. The experiments $3p$ and $4p$ included measurement of the elastic wave velocity U_{el} by means of the contact sensors. The results of measurements of the elastic wave velocity U_{el} are equal or close to the measured c_l under normal pressure. The profiles u_{fs} exhibit a significant difference in behavior of CCCM 1-D in a dependence on the loading direction. If loading along the fibers exhibits a step-wise increase of the free surface velocity due to reflection of the precursor from the plastic wave, then during loading perpendicular to the fiber a monotonic increase of the velocity is recorded, with formation of a pronounced front of the shock wave. When the maximum velocity is reached, irreproducible specific features related to the specimen microstructure are also registered in unloading on the profiles $2p-4p$ A shape of the elastic wave when loading perpendicular to the fibers does not make it possible to calculate an exact value of σ_{HEL}. In the middle part of the elastic wave of the experiments $2p-4p$ its amplitude is 8−9 m/s, which corresponds to $\sigma_{HEL} \sim 14$ MPa. It is by two orders smaller than during shock loading along the fibers. Due to the low velocity c_l, along the direction perpendicular to the fibers we record significant reduction of time Δt between exit of the elastic wave and the plastic wave with an increase of the maximum compression stress. In the experiment $1p$ in Fig. 3, the shock wave velocity exceeded the value of c_l and as a result no elastic-plastic transition is recorded. It was shown by calculating the plastic wave velocity D by the time Δt of exit of the plastic wave that in the experiment $3p$ $D = 1.45$ km/s, in $4p$ — $D = 1.69$ km/s and in $2p$ — $D = 1.79$ km/s. With an increase of the maximum compression stress, the experiments $2p-4p$ exhibit an increase of the strain rate in the plastic wave. Time resolution of the interferometer makes it possible to measure the time of the increase of the velocity in the plastic wave and to evaluate the strain rate by means of the relationship $\dot{\varepsilon} = \dot{u}_{fs}/2D$, where $\dot{u}_{fs}$ is an increase rate of the free surface velocity in the plastic wave. The strain rate in the plastic wave increases from $3.1 \cdot 10^5$ s^{-1} in the experiment $3p$ until $\sim 1.6 \cdot 10^6$ s^{-1} in the experiments $2p$ and $4p$.

The velocity profiles of the free surface $2p-4p$ (Fig. 10) record spall fracture, which is manifested as a minimum in the unloading part of the pulse. The velocity difference designated in the figure as Δu_{fs} makes it possible to determine the value of spall strength [36]. Since fracture is in the plastic area, we use the relationship $\sigma_{sp} = 1/2 \cdot \rho_0 \cdot c_0 \cdot \Delta u_{fs}$ for calculating spall strength. The value of the volume speed of sound during loading perpendicular to the fiber direction is $c_b = 2.170$ km/s. The value of spall strength in the experiments $3p$ and $4p$ was $\sigma_{sp} = 36$ MPa, and in the experiment $2p$ it was $\sigma_{sp} = 110$ MPa. In this case, spall strength does not depend on the maximum compression stress, but it depends on the microstructure, i.e. on a cross section of spallation, inside a fiber or between fibers. The strain rate of the material before spallation is actually a rate of expansion of a substance in the rarefaction wave and is equal to

$$\frac{\dot{V}}{V_0} = -\frac{\dot{u}_{fsr}}{2c_b},$$

where $\dot{u}_{fsr}$ is a rate of drop of the free surface velocity in unloading wave before spallation, which is determined from the wave profile. Table 3 summarizes the obtained values of the strain rates in the rarefaction wave for the experiments along and perpendicular to the fiber direction as well as at the angle of 45° in the plastic area of deformation.

Fig. 11 summarizes the obtained values of spall strength of the CCCM 1-D on the strain rate for the studied orientations. The transparent red dot corresponds to spall strength at longitudinal fiber orientation in the test $1a$. It is clear that within the area of plastic deformation (the solid blue and green dots as well as the transparent red dot) at the strain rates $\sim 10^4$ s^{-1} the values of spall strength for the studied orientations slightly differ from each other and stay within the range 35−70 MPa. In the perpendicular direction, we record a twofold increase of spall strength from an increase of the strain rate by an order. Fig. 11 also shows results of investigation of spall strength of a carbon fiber-reinforced plastic (CFRP) from the study [11], which quantitatively quite well agree with the data obtained. At the same time, it should be noted that the dependences of spall strength on the strain rate do not coincide, but intersect, which is one of manifestations of various influence of the carbon (CCCM 1-D) matrix and the polymer (CFRP) matrix on spall strength of the composites. In loading along the fibers, fracture occurs at the interface between the areas of elastic and plastic deformation. Since the specimen is

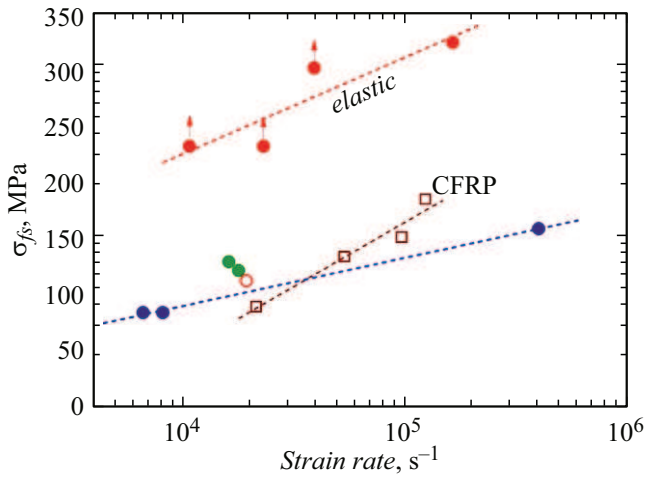

Figure 11. Dependence of spall strength on the strain rate of the CCCM 1-D under shock loading along (the red dots), perpendicular to (the blue dots) and at the angle of 45° (the greed dots) to the fiber direction. CFRP — experimental data from [42].

not fracture in the elastic area, the arrow dots shown in Fig. 11 characterize not spall strength, but the maximum tensile stresses, which were implemented in the elasticity area in a specific test. The respective values are by an order higher than spall strength in the plastic area. This behavior is typical for single-crystal sapphire, in which extremely high values of spall strength are recorded in the elastic area and with a transition into the plastic-flow area the strength becomes to either zero or insignificant. This behavior is typical for some ceramics [36].

Conclusion

We have determined the structure of the front of the shock wave and shock compressibility of the unidirectional carbon-carbon composite material CCCM 1-D during propagation of the shock waves at the angles 0, 45 and 90° in relation to fiber orientation. When loading the specimen along the fibers, we have recorded the two-wave configuration, which is observed within the entire studied pressure range to 40 GPa. The similar structure of the front is observed with fiber orientation at the angle of 45°. But due to a smaller value of c_l the two-wave configuration disappears earlier than at 0°, since the velocity of propagation of the first wave is determined by the speed of sound, which is measured along the fibers. It is demonstrated that the shock Hugoniot of the composite depends on a direction of shock-wave impact. Around the shock compression pressure of 30 GPa the shock Hugoniot registers a kink that indicates the phase transition at this shock compression pressure.

Based on recording and subsequent analysis of the wave profiles, we have measured spall strength of the unidirectional carbon-carbon composite material CCCM 1-D under shock loading of the samples at the angles 0, 45 and 90° in relation to fiber orientation. It is demonstrated that the studied composite is no fracture occurs in the area of elastic deformation, i.e. the value of spall strength is determined by its dynamic elastic limit and exceeds 1 GPa. During plastic deformation, the CCCM 1-D sample loses the elastic properties and spall strength decreases by an order irrespective of fiber orientation. At the same time, a heavy dependence of σ_{sp} on the strain rate is observed, whose increase by an order results in a twofold increase of spall strength.

Funding

Thus study was performed under state assignment of the Ministry of Education and Science of Russia as per the program „Complex research of physical-chemical properties and processes in matter under conditions of high-energy impact“, Federal Research Center for Problems of Chemical Physics and Medical Chemistry, Russian Academy of Sciences, topic No. FFSG-2024-0001, registration No. 124020600049-8 using the equipment belonging to CUC „Promising explosion technologies“ as well as URF (unique research facility) „Experimental explosion bench“.

Conflict of interest

The authors declare that they have no conflict of interest.

References

[1] P.N.B. Reis, J.A.M. Ferreira, Z.Y. Zhang, T. Benameur, M.O.W. Richardson. Compos. Part B Eng., **46**, 7 (2013). DOI: 10.1016/j.compositesb.2012.10.028
[2] D.M. Dattelbaum, J.D. Coe, P.A. Rigg, R.J. Scharff, J.T. Gammel. J. Appl. Phys., **116**, 194308 (2014). DOI: 10.1063/1.4898313
[3] I. Taraghi, A. Fereidoon, F. Taheri-Behrooz. Mater. Des., **53**, 152 (2014). DOI: 10.1016/j.matdes.2013.06.051
[4] E. Zaretsky, G. DeBotton, M. Perl. Int. J. Solids Struct., **41**, 569 (2004). DOI: 10.1016/j.ijsolstr.2003.09.026
[5] D.M. Dattelbaum, J.D. Coe. *The dynamic loading response of carbon-fiber-filled polymer composites*. In V.V. Silberschmidt (editor). *Dynamic Deformation, Damage and Fracture in Composite Materials and Structures* (Woodhead Publishing, 2016), p. 225–277. DOI: 10.1016/B978-0-08-100080-9.00009-9
[6] P.-L. Hereil, O. Allix, M. Gratton. J. Phys., **IV** (7), C3 (1997). DOI: 10.1051/jp4:1997391
[7] V.M. Mochalova, A.V. Utkin, V.E. Rykova, M. Endres, D.H.H. Hoffmann. Arch. Mech., **71**, 417 (2019). DOI: 10.24423/aom.3144
[8] V. Mochalova, A. Utkin, A. Savinykh, G. Garkushin. Compos. Struct., **273**, 114309 (2021). DOI: 10.1016/j.compstruct.2021.114309
[9] S.A. Bordzilovskii, S.M. Karakhanov, L.A. Merzhievskii. Combust. Explos. Shock Waves, **33**, 354 (1997). DOI: 10.1007/BF02671876
[10] J.C.F. Millett, N.K. Bourne, Y.J.E. Meziere, R. Vignjevic, A. Lukyanov. Compos. Sci. Technol., **67**, 3253 (2007). DOI: 10.1016/j.compscitech.2007.03.034

[11] W. Riedel, H. Nahme, K. Thoma. *Equation of state properties of modern composite materials: Modeling shock, release and spallation*. In AIP Conf. Proc. (American Institute of Physics, 2004), p. 701–706, DOI: 10.1063/1.1780335
[12] N. Agarwal, A. Rangamani, K. Bhavsar, S.S. Virnodkar, A.A.A. Fernandes, U. Chadha, D. Srivastava, A.E. Patterson, V. Rajasekharan. Front. Mater., **11**, 1374034 (2024).
[13] T. Lässig, F. Bagusat, S. Pfändler, M. Gulde, D. Heunoske, J. Osterholz, W. Stein, H. Nahme, M. May. Compos. Struct., **182**, 590 (2017). DOI: 10.1016/j.compstruct.2017.09.031
[14] B.X. Bie, J.H. Han, L. Lu, X.M. Zhou, M.L. Qi, Z. Zhang, S.N. Luo. Compos. Part Appl. Sci. Manuf., **68**, 282 (2015). DOI: 10.1016/j.compositesa.2014.10.001
[15] A.V. Bushman, V.P. Efremov, V.E. Fortov, G.I. Kanel, I.V. Lomonosov, V.Y. Ternovoi, A.V. Utkin. Shock Compression Condens. Matter, **1991**, 79 (1992). DOI: 10.1016/B978-0-444-89732-9.50018-2
[16] P.J. Hazell. Dyn. Deform. Damage Fract. Compos. Mater. Struct., **337** (2016). DOI: 10.1016/B978-0-08-100080-9.00012-9
[17] J. Ribeiro, I. Plaksin, J. Campos, R. Mendes, J. Gois. *Process of shock attenuation inside a hollow glass microsphere/polymeric composite media*. In: AIP Conf. Proc. (American Institute of Physics, 2000), p. 559–562, DOI: 10.1063/1.1303536
[18] R.F. Trunin, L.F. Gudarenko, M.V. Zhernokletov, G.V. Simakov. *Experimental data on shock compression and adiabatic expansion of condensed matter* (RFNC-VNIIEF, Sarov, 446, 2001)
[19] S. Katz, E. Zaretsky, E. Grossman, H.D. Wagner. Compos. Sci. Technol., **69**, 1250 (2009). DOI: 10.1016/j.compscitech.2009.02.031
[20] D.M. Dattelbaum, J.D. Coe. Polymers, **11**, 493 (2019). DOI: 10.3390/polym11030493
[21] T.A. Rostilov, V.S. Ziborov. Acta Astronaut., **178**, 900 (2021). DOI: 10.1016/j.actaastro.2020.10.022
[22] V.M. Mochalova, A.V. Utkin, A.V. Pavlenko, S.N. Malyugina, S.S. Mokrushin. Tech. Phys., **64** (1), 100 (2019). DOI: 10.1134/S1063784219010225
[23] R.C. Huber, J. Peterson, J.D. Coe, D.M. Dattelbaum, L.L. Gibson, R.L. Gustavsen, J.M. Lang, S.A. Sheffield. J. Appl. Phys., **127**, 105902 (2020). DOI: 10.1063/1.5124252
[24] J.C.F. Millett, N.K. Bourne, N.R. Barnes. J. Appl. Phys., **92**, 6590 (2002). DOI: 10.1063/1.1506389
[25] S.A. Bordzilovskii, S.M. Karakhanov, K.V. Khishchenko. Explos. Shock Waves, **49**, 121 (2013). DOI: 10.1134/S0010508213010140
[26] C.S. Alexander, C.T. Key, S.C. Schumacher. J. Appl. Phys., **114**, 223515 (2013). DOI: 10.1063/1.4846116
[27] D.C. Wood, G.J. Appleby-Thomas, A. Hameed, N.R. Barnes, A. Hughes, P.J. Hazell. J. Mater. Sci., **53**, 11415 (2018). DOI: 10.1007/s10853-018-2431-0
[28] N.K. Bourne, S. Parry, D. Townsend, P.J. Withers, C. Soutis, C. Frias. Philos. Trans. R. Soc. Math. Phys. Eng. Sci., **374**, 20160018 (2016). DOI: 10.1098/rsta.2016.0018
[29] S. Shah, P.J. Hazell, H. Wang, J.P. Escobedo. Compos. Part B Eng., 112438 (2025).
[30] S. Shah, P.J. Hazell, H. Wang, J.P. Escobedo. *Shock Wave Propagation in Unidirectional CFRP at Different Orientations*. In Hypervelocity Impact Symp. (American Society of Mechanical Engineers, 2024), p. V001T07A002, https://asmedigitalcollection.asme.org/hvis/proceedings-abstract/HVIS2024/88728/1218760 (accessed June 30, 2025)
[31] V. Mochalova, A. Utkin, D. Nikolaev. J. Appl. Phys., **133**, 245902 (2023). DOI: 10.1063/5.0155414
[32] V. Mochalova, A. Utkin, V. Sosikov, V. Yakushev, A. Zhukov. Shock Waves, **32**, 715 (2022). DOI: 10.1007/s00193-022-01104-3
[33] L.M. Barker, R.E. Hollenbach. J. Appl. Phys., **43**, 4669 (1972). DOI: 10.1063/1.1660986
[34] G.I. Kanel, A.S. Savinykh, G.V. Garkushin, S.V. Razorenov. *Re-Reflections of an Elastic Precursor of a Shock Wave in Solids*. In Dokl. Phys. (Springer, 2021, p. 35–38), https://idp.springer.com/authorize/casa?redirect_uri=https://link.springer.com/article/10.1134/S1028335821020038&casa_token=m67TQmSjhdMAAAAA:GhxsibO7f4jjtGw2HI5VZBEKP9uxR_FcwUqUuxuuXSDX9TtPjUFYTmtgd8S0VeAYRkUVv1XgTdDyhj_Ci0I (accessed April 23, 2025).
[35] G.I. Kanel, *Udarnye volny v fizike tverdogo tela* (Fizmatlit, M., 2018) (in Russian). https://www.rfbr.ru/library/books/2814/ (accessed November 24, 2025).
[36] G. Kanel, S. Razorenov, A. Utkin, V. Fortov. *Shock-Wave Phenomena in Condensed Media* (Yanus-K, M., 1996)
[37] D.J. Erskine, W.J. Nellis. J. Appl. Phys., **71**, 4882 (1992).
[38] D.J. Erskine, W.J. Nellis. Nature, **349**, 317 (1991).
[39] N.A. Zlatin, S.M. Mochalov, G.S. Pugachev, A.M. Bragov. ZhTF, **45** (3), 681 (1975) (in Russian).
[40] N.A. Zlatin, G.S. Pugachev, S.M. Mochalov, A.M. Bragov. FTT, **17**, 2599 (1975) (in Russian).
[41] S.A. Novikov, I.I. Divnov, A.G. Ivanov. Fizika metallov i metallovedenie, **21**, 608 (1966) (in Russian).
[42] W. Xie, W. Zhang, L. Guo, Y. Gao, D. Li, X. Jiang. Compos. Part B Eng., **153**, 176 (2018).

Translated by M.Shevelev